Sensitivity analysis of a physicochemical model of chloride ingress into real concrete structures subjected to long-term exposure to tidal cycles

Nicolas Reuge, François Bignonnet, Stéphanie Bonnet

Applied Ocean Research 138 (2023), https://doi.org/10.1016/j.apor.2023.103622

Sensitivity analysis of a physicochemical model of chloride ingress into real concrete structures subjected to long-term exposure to tidal cycles

Nicolas Reuge[a], François Bignonnet[a], Stéphanie Bonnet[a,*]

[a]Nantes Université, Ecole Centrale Nantes, CNRS, GeM, UMR 6183 F-44600, Saint-Nazaire, France

[*]Corresponding author – email: stephanie.bonnet@univ-nantes.fr

Abstract

In marine environments, reinforced concrete structures are exposed to tidal conditions and therefore susceptible to chloride ingress. Reliable models of transport are crucial in order to evaluate the service life of these structures. Unlike engineering models based on Fick's 2nd law and empirical coefficients, this study proposes a model based on a physicochemical description of the transport phenomena and on some assumptions restricting the number of inputs to 9 parameters and the computational costs. This model is validated for a long exposure to tidal cycles (28 years). Then, the sensitivity analysis, based on the Morris method, is performed through 100 simulations of tidal exposure considering different sets of the 9 input parameters. According to the critical times of initiation of corrosion predicted, the most sensitive parameters are the critical chloride concentration and the chloride diffusivity factors. The effects of moisture sorption and chloride binding parameters are moderate after long exposure. Then, the results of the simulations are compared to data of the literature in terms of convection depths and total chloride concentrations at the limit of the convection / diffusion zones. Finally, by quantitative considerations, the analysis goes further, providing analytical relations expressing the convection depth and the associated total chloride concentration as functions of input parameters. These provide physically informed guidelines in using an engineering model based on Fick's 2nd law in order to estimate the critical time of initiation of corrosion.

Keywords: Reinforced concrete, Chloride ingress, Tidal conditions, Long exposure, Modeling, Sensitivity analysis

1 Introduction

Chloride-induced corrosion of RCs (Reinforced Concretes) in marine environments is of major concern (Al-Rabiah et al, 1990; Bao et al., 2022). This is especially the case for structures subjected to tidal or splashing conditions (Al-Rabiah et al, 1990; Bao et al.,2022, Chen et al., 2022) such as offshore structures, buildings, bridges and quays. In conditions of immersion, chloride ions are transported by water, they penetrate deeper and deeper into the concrete porosity and can bind to the material. In conditions of emersion, bound chlorides progressively accumulate. Cycle after cycle, chlorides penetrate to the rebars, their quantity progressively increases to a critical concentration allowing the initiation of corrosion (Angst et al., 2009). Corrosion of rebars promotes cracking and thus damages the whole concrete structures (Al-Rabiah et al, 1990; Tian et al., 2020; Qu et al., 2021) involving short service life and potentially high costs of restoration (Truong et al, 2022).

Given the challenges of marine concrete structures, the related impacts of global warming and climate change are likely to be among the most severe issues. Global temperatures and sea levels are

raising, and extreme weather events have increased. When they affect coastal infrastructure, they are incredibly destructive (Qu et al., 2021).

The French DEMCOM Project funded by the French National Research Agency was undertaken in order to minimize the environmental impacts and costs and to maximize the durability of marine RC structures (Bonnet et al., 2022). In this frame, it is crucial to understand the mechanisms involved in chloride transport in order to develop models able to predict durability of exposed structures. Such transport models can then be coupled with life cycle assessment (LCA) to optimize concretes formulations.

Transport models of chloride ions into concretes are available in literature and can be divided into three categories:

- engineering models based on the Fick's 2nd law, possibly associated with a probabilistic approach such as the one provided by the "fib model code", detailed in (Gelhen et al., 2015),

- artificial Neural Networks (ANN) and machine-learning based models, as recently developed by Liu et al. (2021, 2022),

- physicochemical models based on a detailed description of the transport phenomena involved (Sleiman, 2009; Baroghel-Bouny, 2011; Achour et al., 2019; Li et al., 2022).

These three approaches are useful. Engineering models are simple to implement and lead to rapid results. On one hand, by simply using the Fick's 2nd law, they ignore some hygric and advective phenomena and thus some materials properties that can actually have an effect on chloride ingress. On the other hand, physicochemical models require the knowledge of some input parameters which can be difficult to determine experimentally.

Now, the question is to determine the sensitivity of the chloride ingress to these different parameters and properties. Various SA (Sensitivity Analysis) studies have already been carried out on chloride ingress inside cement concrete. Boddy et al. (1999) used a One At a Time (OAT) technique for sensitivity investigation of a chloride transport model to the variations of the parameters controlling the rate of diffusion, temperature of exposure, critical chloride level, diffusion coefficient, permeability coefficient, surface chloride concentration and position of steel rebar. Kirkpatrick et al. (2002) studied a probabilistic model to predict the initiation of chloride corrosion depending on the position of the steel rebar, surface chloride concentration and apparent diffusion coefficient. A deeper deterministic study than the two previous ones was conducted by Zhang and Lounis (2006) undertaking a differential analysis method on corrosion model depending on four governing parameters: apparent chloride diffusion coefficient, position of steel rebar, surface chloride concentration and chloride threshold. Bao et al. (2022) performed a parametric SA to study the effects of the cyclic drying-wetting ratio and of the initial liquid saturation degree of concrete pores. Ta et al. (2016) have applied successively Morris and Sobol approaches as complementary methods for sensitivity analysis of a carbonation model. Based on this study, Kiesse et al. (2020) also used Morris and Sobol approaches for sensitivity analysis of a diffusion-based chloride transport model. Their work went beyond the previous studies on uncertainties in the models describing the degradation of reinforced concrete structures, by considering the individual influence of available input parameters as well as the influence of their interaction on model output; however, only

transport by diffusion and constant boundary conditions (i.e., engineering approach) were taken into account.

All these previously cited studies were based on over-simplified transport descriptions or boundary conditions. In the present study, a sensitivity study based on a physicochemical approach is proposed taking into account hygric phenomena and realistic tidal exposure conditions. Note that such a study has not been done before, in part because of the computational costs that it involves. To keep reasonable computational times for the sensitivity analysis, it is assumed in the present study that concrete can be represented as a homogeneous material at the structure scale. Hence, heterogeneities such as aggregates, interfacial transition zones or cracks are not explicitly accounted for in the simulations unlike in the works of Liu et al. (2015), Wang et al. (2016) or Tong et al. (2023). Their contribution is implicitly taken into account through the material properties.

First, preliminary considerations and constitutive relationships will be given. Then, based on some justified assumptions, the governing equations of the physicochemical approach will be detailed. This detailed approach will be confronted to chloride ingress through tidal / splashing on-site measurements. The main step of the study will consist in performing a SA by Morris method on properties of a material subjected to relevant tidal conditions. Then, from the information provided by the sensitivity analysis, analytical expressions of the convection depth and chloride concentration at this depth will be deduced as function of the input parameters. Finally, using these expressions, a new engineering model based on the 2nd law of Fick will be given and tested.

2 Governing equations of hygric and chloride transport in unsaturated concrete

Chloride ions transport in an unsaturated concrete is ruled by convection (i.e., liquid pressure gradient) and diffusion (i.e., chloride content gradient). Theoretical descriptions have already been given in (Baroghel-Bouny et al., 2011) and (Achour et al., 2019), but synthetical formulations will be given here based on some justified assumptions.

2.1 Assumptions and constitutive relationships

2.1.1 Liquid phase transport

As shown by Thiery et al. (2007) for drying of concrete samples, from a purely hygric point of view, transport of gas phase can be neglected: provided that the ambient Relative Humidity (*RH*) remains greater than about 50%, transport is ruled by the Darcy flow of the liquid phase. Actually, coupling Cl ions transport with the hygric problem does not change the validity of this assertion: preliminary calculations of chloride ingress into concrete exposed to tidal conditions have been performed and have shown that transport of gas phase (water vapor and air) could be neglected (Reuge et al., 2023).

Therefore, inside the porous materials, the gas phase (*g*) is considered as motionless and the liquid phase (*l*) is liquid water (*w*) which contains Cl ions. The volumetric ratio of liquid water in the concrete open porosity φ is called degree of saturation S_l. In the depth of the porous material (Cartesian coordinate *x*), the velocity of the liquid phase is described by the Darcy's law (i.e., viscous flow) (Kast and Hohenthanner, 2000):

$$v_l = -\frac{K k_{r,l}(S_l)}{\eta_l}\frac{\partial P_l}{\partial x} \quad (1)$$

where η_l is the dynamic viscosity of phase *l*, *K* and $k_{r,l}$ are the intrinsic and relative permeabilities respectively. Relative permeability depends on some concrete properties and on S_l and on the adsorption / desorption state of the liquid phase (Baroghel-Bouny et al., 2011).

Whatever the porous material, its water sorption as a function of local relative humidity H_r is commonly described by the Van Genuchen (VG) model (Van Genuchten, 1980) used by many authors to describe the moisture transport in concretes (Mainguy, 1999; Thiery et al., 2007; Kameche et al., 2014, Bonnet and Balayssac, 2018). It is expressed as follows:

$$S_l(Hr) = \left[1 + \left(-\frac{\rho_w RT}{M_w}\cdot\frac{1}{a}\ln(Hr)\right)^{\frac{1}{1-m}}\right]^{-m} \quad (2)$$

where H_r is by definition equal to $P_v/P_{v,\text{sat}}$, P_v is the vapor pressure and $P_{v,sat}$ is given by the Clausius-Clapeyron equation (Atkins, 1985). *a* (Pa) and *n* (-) are VG coefficients adjustable on measurements. Note that these coefficients can have significantly different values in adsorption and desorption conditions because adsorption and desorption isotherms differ.

The relation between liquid and gas total pressures is given by:

$$P_l = P_g - P_c(S_l) \quad (3)$$

where P_g is considered constant and equal to atmospheric pressure P_{atm} and P_c is the capillary pressure which can be well estimated by the following equation involving the VG coefficients from eq. (2) and Kelvin's law (Van Genuchten, 1980):

$$P_c(S_l) = a\left(S_l^{-1/m} - 1\right)^{1-m} \quad (4)$$

According to (Van Genuchten, 1980), liquid relative permeability can be estimated by the following equations:

$$k_{r,l}(S_l) = S_l^{1/2}\left[1 - \left(1 - S_l^{1/m}\right)^m\right]^2 \quad (5)$$

Actually, eq. (5) is only valid in adsorption conditions. In desorption conditions, $k_{r,l}$ can be determined by a complex method involving integrations of capillary pressure expressions as described in (Baroghel-Bouny et al., 2011; Kameche et al., 2014).

2.1.2 Chloride ions transport

Chloride ions transport occur in liquid water. A part of these ions can be adsorbed by physisorption and chemisorption inside the material, these bound chlorides are considered as motionless. Chloride concentration will be noted c_{Cl} (mol.m^{-3} of solution) or C_{Cl} (mol.m^{-3} of concrete).

The effective diffusivity of free chloride ions D_{eff} in the liquid phase of an unsaturated porous medium can be modeled as follows (Buchwald, 2000; Bao et al., 2022):

$$D_{eff}\left(S_l\right) = D_{eff,0} S_l^{\lambda} \tag{6}$$

where $D_{eff,0}$ is the Cl ions diffusivity in the saturated porous medium (which can be measured, see (Ben Fraj et al., 2012)) and λ is an adjustable exponent. From adjustments of simulations on experiments (Baroghel-Bouny et al., 2011), a value of 6 has been obtained for λ.

Finally, free Cl ions concentration $c_{Cl,f}$ (mol.m^{-3} of solution) and bound Cl concentration $C_{Cl,b}$ (mol.m^{-3} of concrete) are linked by binding isotherms. Binding is described by the following law:

$$C_{Cl,b}\left(c_{Cl,f}\right) = C_{Cl,p}\left(c_{Cl,f}\right) + C_{Cl,c} = \mu\left(c_{Cl,f}\right)^{\gamma} + 2n_{eq} \tag{7}$$

where $C_{Cl,p}$ and $C_{Cl,c}$ are physisorbed and chemisorbed Cl concentrations respectively. The first term corresponds to the model of Freundlich for Cl physisorption, its coefficients μ and γ can be determined experimentally (see (Ben Fraj et al., 2012)). A part of Cl ions can be bound by chemisorption (i.e., the second term) to form Friedel salts according to the aluminate equivalent of the material n_{eq} (Baroghel-Bouny et al., 2011).

It is important to note that the binding law (7) is theoretically only valid when the open porosity of the material is saturated with water (i.e., $S_l = 1$). Nothing has been found in literature regarding the case of unsaturated materials. It is proposed here to take this into account using the following law:

$$C_{Cl,b}\left(c_{Cl,f}, S_l\right) \quad = \mu\left(S_l^{\beta} c_{Cl,f}\right)^{\gamma} + 2n_{eq} \tag{8}$$

where β is an adjustable exponent between 0 (i.e., Eq. (7)) and 1.

For the approach presented here, Cl is assumed as the only ionic species. Multispecies approaches are available in literature (Wang, 2012; Soive et al., 2018; Achour et al., 2019) but the interaction of Cl with other ions seems to be of minor importance compared to the other transport mechanisms (i.e., advection and diffusion) (Wang, 2012). Moreover, multispecies approaches require the knowledge of ionic concentrations in the initial pore solution: they significantly depend on the concrete formulation which implies additional assumptions and sources of uncertainty.

Effects of carbonation are ignored as ambient relative humidity *RH* close to marine structures is rarely below 80%: this limits the carbonation process very significantly as explained by Ta et al. (2016). Moreover, the model of Achour (2018) has shown that the effect of carbonation on concrete structural properties in tidal conditions is quite small, too small to significantly modify hygric and ionic transports.

2.2 Mass balance equations

The mass balance equations expressed in molar form lead to the following system:

$$\begin{cases} \dfrac{\partial}{\partial t}\left(\varphi S_l\right) - \dfrac{\partial}{\partial x}\left[\dfrac{K k_{r,l}}{\eta_l}\dfrac{\partial P_l}{\partial x}\right] = 0 \\ \dfrac{\partial}{\partial t}\left(\varphi S_l c_{Cl,f} + C_{Cl,b}\right) - \dfrac{\partial}{\partial x}\left[D_{eff}\dfrac{\partial c_{Cl,f}}{\partial x} + c_{Cl,f}\dfrac{K k_{r,l}}{\eta_l}\dfrac{\partial P_l}{\partial x}\right] = 0 \end{cases} \tag{9,10}$$

Equation (9) describes the liquid water transport (unknown: S_l) and equation (10) describes the transport of free chloride ions (unknown: $c_{Cl,f}$). The closure relations are given by eqs. (3), (4) and (8). Note that the process of Cl binding is considered here as instantaneous (according to the binding isotherm).

2.3 Kinetics of binding

Actually, Cl binding by physisorption is not instantaneous and a kinetics of physisorption should be considered. In contrast, Cl binding by chemisorption is much more rapid and can be considered as instantaneous. From (Baroghel-Bouny et al., 2011), the kinetics of physisorption is of an order of 1 and eq. (10) is therefore replaced by the following equations:

$$\begin{cases} \dfrac{\partial}{\partial t}\left(\varphi S_l c_{Cl,f} + C_{Cl,c}\right) - \dfrac{\partial}{\partial x}\left[D_{eff} \dfrac{\partial c_{Cl,f}}{\partial x} + c_{Cl,f} \dfrac{K k_{r,w}}{\eta_l} \dfrac{\partial P_l}{\partial x} \right] = -k_0 \left(C_{Cl,p}^{eq} - C_{Cl,p} \right) \\ \dfrac{\partial}{\partial t}\left(C_{Cl,p} \right) = k_0 \left(C_{Cl,p}^{eq} - C_{Cl,p} \right) \end{cases} \quad (11,12)$$

with:

$$\begin{cases} C_{Cl,p}^{eq} = \mu \left(S_l^{\beta} c_{Cl,f} \right)^{\gamma} \\ C_{Cl,c} = 2 n_{eq} \end{cases} \quad (13,14)$$

k_0 is a kinetic constant and can be expressed using a characteristic time τ of physisorption:

$$k_0 = 1/\tau \quad (15)$$

To conclude this part, it is useful to consider the list of all the parameters intrinsic to the concrete appearing in the equations: the open porosity φ, the permeability K, the VG parameters a and m, the binding parameters μ, γ, β and n_{eq}, the chloride diffusion parameters $D_{eff,0}$ and λ and the characteristic time τ if the kinetics of physisorption is taken into account. From this list, 2 parameters (n_{eq} and τ) can be removed if Cl chemisorption and Cl binding kinetics of physisorption are ignored.

3 Model validation and quantification of the effects of simplifications

3.1 Materials properties

For preliminary simulations, the mortar M1N (Bonnet and Perrin, 1999) and the Ordinary Portland Cement Concrete OPCC60 (Ben Fraj et al., 2012) have been chosen. Their compositions are given in the aforementioned references. The properties of the mortar M1N have been very thoroughly investigated in previous studies (Francy and François, 1998a; Bonnet and Perrin, 1999; Baroghel-Bouny et al., 2011) so this mortar is the ideal candidate to begin this study. OPCC60 is a rather common concrete and its properties have been investigated in laboratory by Ben Fraj et al. (2012) and a similar one on-site by Othmen et al. (2018). The properties of these two compounds are given in Table 1.

	φ (-)	Sorption a (Pa) – ads./des.	Sorption m (-)	Binding μ	Binding γ (-)	Binding n_{eq} (mol.m^{-3})	K (m^2)	$D_{eff,0}$ (m^2.s^{-1})
M1N	0.13	11.10^6 / 25.10^6	0.49	2.61	0.61	5.25	6.10^{-20}	2.10^{-12}
OPCC60	0.14	$4.75.10^6$ / -	0.4	3.5	0.69	-	3.10^{-20}	$0.7.10^{-12}$

Table 1: Properties of mortar M1N (Francy and François, 1998a; Bonnet and Perrin, 1999; Baroghel-Bouny et al., 2011) and of concrete OPCC60 (Ben Fraj et al., 2012; Othmen et al., 2018)

Regarding M1N, adsorption and desorption isotherms have been experimentally determined by Bonnet and Perrin (1999). In adsorption conditions, experimental points and adjustments with VG model are shown in Figure 1a. Regarding Cl binding, measurements and adjustment with model (7) are shown in Figure 1b. The value of K of 6.10^{-20} m^2 showed in Table 1 has been determined here from numerical adjustments of the model on experiments of drying and imbibition carried out by Francy (1998b).

Regarding OPCC60, only the adsorption isotherm has been experimentally determined by Ben Fraj et al. (2012), experimental points and adjustment with VG model are shown in Figure 1a. As shown in Figure 1b, measurements of binding performed in (Ben Fraj et al., 2012) were far to be numerous enough at low $c_{Cl,f}$ to estimate n_{eq}, consequently, it was ignored. The value of K is actually not known for this material, a typical value of 3.10^{-20} m^2 for ordinary Portland cement concrete (Bamforth, 1987) is considered preliminarily.

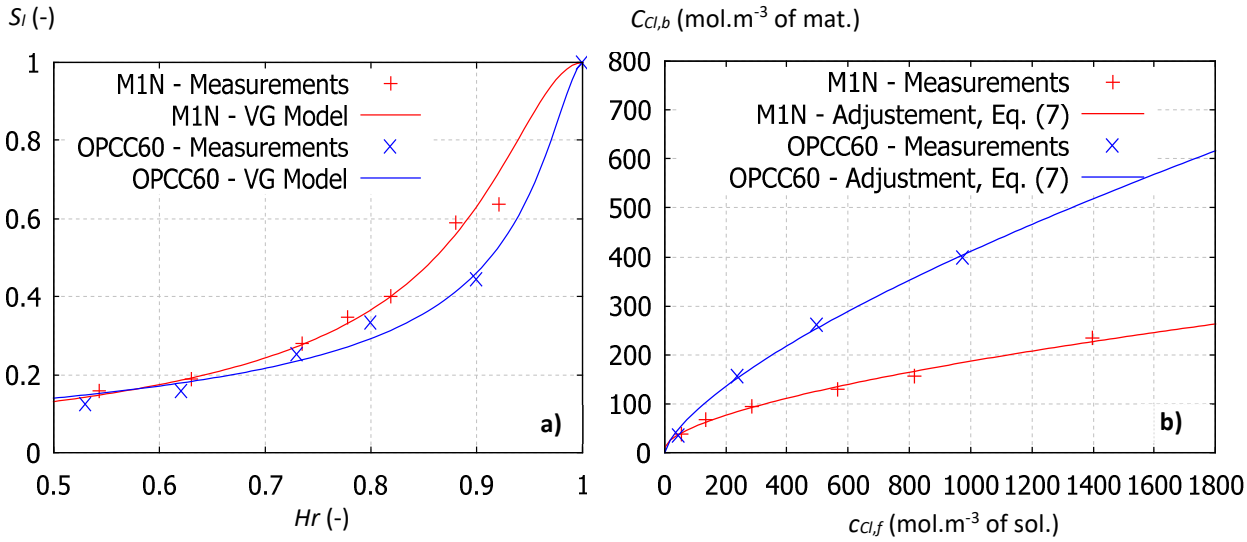

Figure 1: Mortar M1N and concrete OPCC60, (a) isotherms of adsorption – measurements (Bonnet and Perrin, 1999; Ben Fraj, 2012) and adjustments with the VG model, (b) binding isotherms – measurements (Bonnet and Perrin, 1999; Ben Fraj, 2012) and adjustments.

3.2 Simulations in tidal conditions and validation for long exposure

The models have been implemented in a finite element solver platform called FlexPDE®. Its solver is based on a modified Newton-Raphson iteration procedure. Meshes were generated automatically

and during the calculations, refinement was adaptative, but broadly, they never exceeded 100 nodes. Timestep was also adaptative.

For tidal simulations, the exposed face of the materials was considered alternately immersed / emerged for cycle durations of 6 h / 6 h respectively which led to a periodicity of 12 h. The 6h / 6h cycle corresponds to the middle tide zone. Other cycles such as 3h / 9h or 9h / 3h can be encountered in other tide zones. However, since the main focus of this work is to study the sensitivity regarding the materials parameters and not environmental ones, only 6h / 6h cycles are considered here.

Average temperature *T* of 13°C and *RH* of 80% in air have been reported by Othmen et al. (2018) and considered as constant for the simulations. A depth *L* of 10 cm was considered for the materials: this dimension has been chosen to be far beyond the position of the reinforcement for a RC structure exposed to a maritime environment (EN 206-1, 2004; EN 1992-1-1, 2005).

Excepted in section 3.2.4, adsorption isotherms and relative liquid permeabilities of adsorption were considered over the full cycles. Excepted in section 3.2.3, Cl binding was considered as instantaneous.

3.2.1 Boundary and initial conditions

In fully immersed conditions, the material was considered as exposed to RH_{max} of 99.9%. In fully emerged conditions, RH_{min} was fixed at 80%, which corresponds to the external relative humidity recorded by the French Government weather station near the Saint-Nazaire harbor (cf. www.infoclimat.fr). Actually, transitions between immersed / emerged states were not considered as instantaneous. Figure 2a shows *RH* (or *Hr* at the material surface) over a full period (i.e., 0 h - 12 h). In the time range [0, 6h], a progressive temporal evolution of *RH* is given by the following purely theoretical function:

$$RH\left(t\right)=Hr\left(x=0,t\right)=RH_{\max}-\left(RH_{\max}-RH_{\min}\right)\frac{\tanh\left[b_0\left(t-c_0\right)/t_{month}+a_0\right]-\tanh\left(a_0\right)}{\tanh\left[b_0\left(6-c_0\right)/t_{month}+a_0\right]-\tanh\left(a_0\right)} \quad (16)$$

with: a_0 = 18.33, b_0 = -5686.67, c_0 = 0.647 h and t_{month} = 729.98 h (number of hours in a month of 30.416 days). The symmetrical function is used for temporal evolution of *RH* in the time range [6h, 12h] and this scheme is repeated for the next periods.

As S_l is used as an unknown, the temporal evolution at the material surface is given by:

$$S_l\left(x=0,t\right)=S_l\left[RH\left(t\right)\right] \quad (17)$$

where *RH*(*t*) is given by the just aforementioned scheme and $S_l(RH)$ is given by the VG model.

In immersed conditions, $C_{Cl,f}(x = 0)$ was fixed at a typical sea water chloride concentration $c_{Cl,sea}$ of 598 mol.m^{-3}. On the unexposed side of the sample ($x = L$ = 10 cm), no flux boundary conditions were imposed: this corresponds to conditions found in the core of a structural element. Note that a beam of quay is about 30 cm wide (Othmen et al., 2018).

Initial liquid saturation degree inside the material S_{l0} was fixed to 0.8. Initial $C_{Cl,f}$ was set to zero (excepted in section 3.2.5).

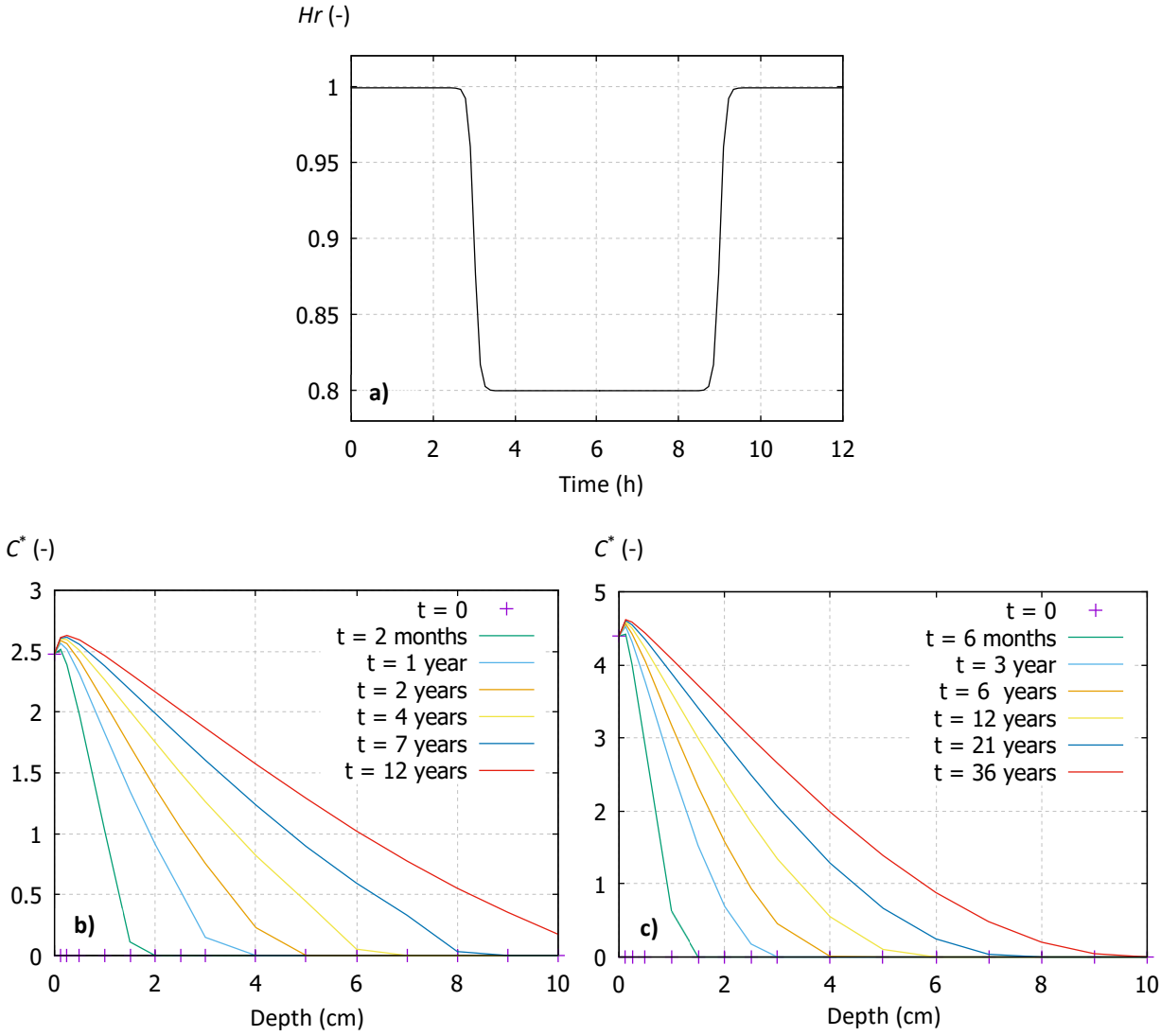

Figure 2: (a) Temporal evolution of *RH* in tidal condition, given by eq. (16), (b) mortar M1N and (c) concrete OPCC60 – profiles of C^* predicted by simulations at different times.

3.2.2 Results

Simulations of tidal cycles have been performed for physical times of 12 years and 36 years for M1N and OPCC60 respectively. Total chloride content $C_{Cl,tot}$ and normalized chloride concentration C^* are defined as follows:

$$\begin{cases} C_{Cl,tot} = \varphi S_l c_{Cl,f} + C_{Cl,b} \\ C^* = C_{Cl,tot} \Big/ \left(\varphi c_{Cl,sea}\right) \end{cases} \tag{18,19}$$

Actually, C^* represents an "enrichment ratio", if the concrete porosity is saturated with sea water at $c_{Cl,sea}$ chloride concentration and in the absence of bound chloride, C^* is equal to 1.

For M1N material, profiles of C^* (in the depth of the materials) at different times obtained from the simulations have been reported in Figure 2b. Note that the points in this Figure correspond to

averaged values of C^* on one cycle of 12h at the following depths: 0 mm, 1.25 mm, 2.5 mm, 5 mm, 1 cm and every cm to 10 cm. These positions being tight close to the exposed surface, the peak position can be estimated quite precisely. According to these results, the position of the chloride content peak evolves from about 1.25 mm during the first years of exposition to about 2.5 mm after 7 years. For OPCC60 material, profiles of C^* at different times obtained from the simulations have been reported in Figures 2c. It appears that the position of the chloride content peak evolves from 1.25 mm to 2.5 mm after 36 years of exposition.

Actually, these predicted positions of the peaks of C^* (at a few mm depths) are in agreement with earlier simulation results obtained by Achour (2018) and Bao et al. (2022). Experimental analysis of samples usually shows much deeper peaks (around 1 cm to 2 cm) (Othmen et al., 2018). The reasons of these discrepancies will be discussed later (see section 3.2.5).

Note that these simulations lasted for about 1 h per year of physical time. Timesteps evolved between 40 s and 45 min as a function of the tidal state.

3.2.3 Effects of binding

An additional simulation of tidal cycles has been performed considering no binding (i.e., $C_{Cl,b} = 0$) for illustration purposes. For M1N, Figure 3a show the temporal evolution of C^* at 2 cm and 5 cm depths. It appears that C^* always remains lower than 1. These results are very interesting because they show that there is no enrichment if chloride binding is ignored. Actually, the enrichment phenomenon reveals to be a combination of tidal cycles (saturation / desaturation) and Cl binding.

As explained in section 2.3, Cl binding by physisorption is not instantaneous compared to the other mass balance terms. For M1N, the characteristic time of physisorption τ is estimated to 5.55 h (Baroghel-Bouny et al., 2011). Thus, a simulation has been performed taking into account this kinetics of physisorption via eqs. (11-15). Figure 3b allows to compare the temporal evolution of C^* at 2 cm and 5 cm depths obtained with / without kinetics of binding. As a result, the kinetics of binding tends to increase C^* but in the moderate extent of 0.2 at maximum. There is no available reference about the characteristic time of physisorption for other compounds, this point should be investigated in the future. The next simulations in this study will be performed considering instantaneous chloride binding.

3.2.4 Effects of adsorption / desorption isotherms and relative liquid permeabilities

In the previous simulations of tidal cycles, adsorption isotherms and relative liquid permeabilities of adsorption were considered over the full cycles. It seems interesting to study the effect of considering the desorption isotherm and the relative liquid permeability of desorption for M1N since they are known.

Simulations have been done considering the desorption isotherm or the relative permeability of desorption over the full cycles (data for relative liquid permeability of desorption given in (Baroghel-Bouny et al., 2011)). Figure 4 allows to compare the temporal evolution of C^* at 2 cm and 5 cm depths for these new simulations with the previous one: it shows that the discrepancies between these simulations always remain lower than 0.2. So, the next simulations in this study will be performed considering only sorption isotherms and liquid relative permeabilities of adsorption.

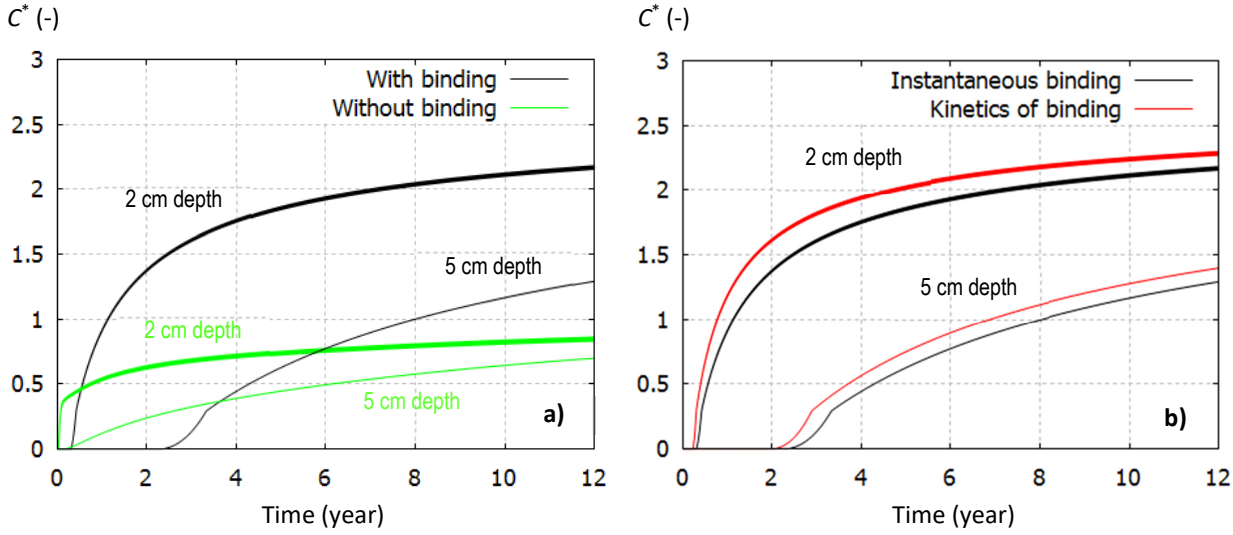

Figure 3: Mortar M1N – temporal evolutions of C^* obtained by the simulations with tidal conditions at 2 cm and 5 cm depths: (a) with / without Cl binding, (b) considering an instantaneous binding / a binding kinetics.

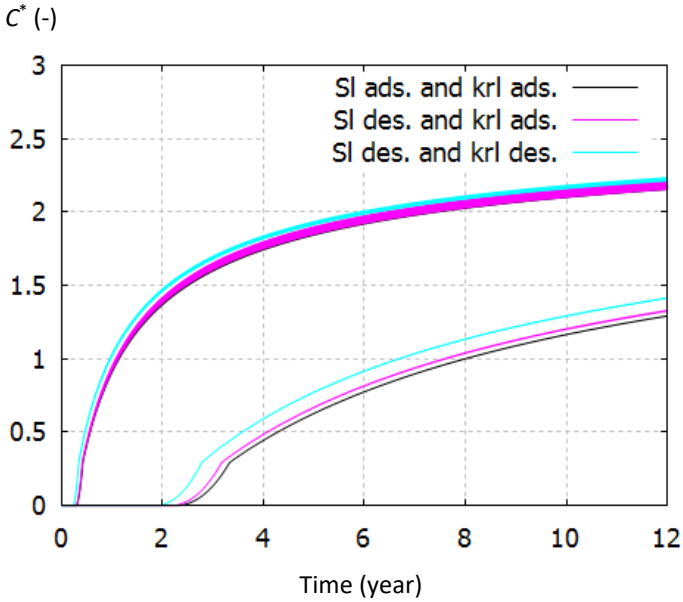

Figure 4: Mortar M1N – temporal evolutions of C^* obtained by the simulations with tidal conditions at 2 cm and 5 cm depths, considering isotherms of adsorption or desorption and liquid relative permeability of adsorption or desorption.

3.2.5 Comparison with measurements and effects of various parameters

In (Othmen et al., 2018), the authors have extracted and analyzed samples of a concrete similar to OPCC60 from a beam exposed to tide and to splashing during 28 years. The studied beam is shown in Figure 5. Note that splashing is known as being as much "aggressive" as tidal cycles (Cai et al., 2020).

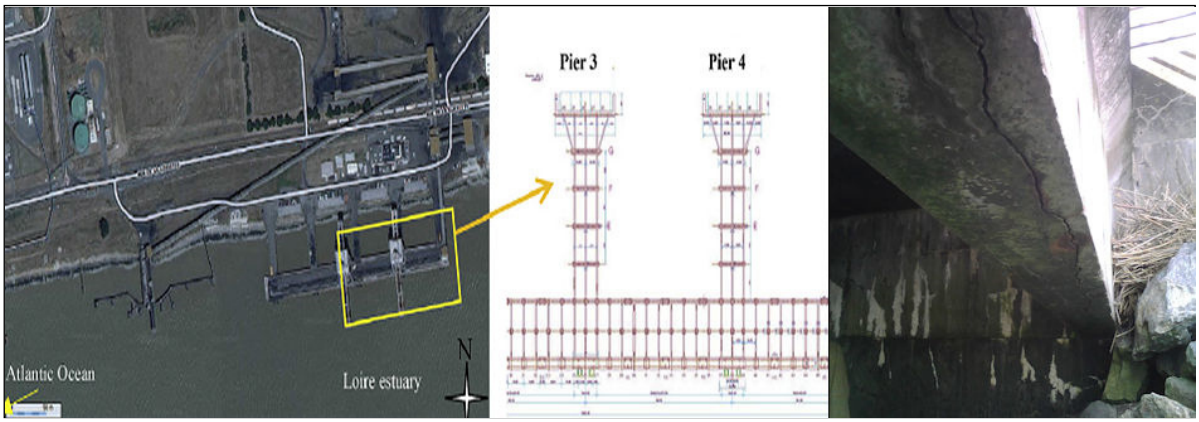

Figure 5: Concrete beam in the Loire estuary analyzed by Othmen et al. (2018).

Thus, 6h / 6h tidal cycles are still considered for the simulations. Moreover, since the authors measured a non-zero concentration of chloride in the concrete core far from the exposed surface, this concentration of 58 mol per m^3 of material is chosen as initial Cl concentration.

Figure 6a shows the C^* averaged profile measured in (Othmen et al., 2018) (average over several samples in the exposed zone) and the results of the simulations performed considering two "extreme" values of K of 10^{-21} m^2 and 10^{-19} m^2 and a value of β of 0 (i.e., no effect of the partial saturation on Cl binding), after 28 years of exposition. First, it appears that the two calculated profiles are very close and therefore the actual value of K is of minor importance under these operating conditions. Figure 6b shows S_l profiles obtained for several values of K: the depth of the convection zone, here defined as the depth at which the saturation profile is stabilized, varies from about 2.5 mm (with $K = 10^{-21}$ m^2) to about 1 cm (with $K = 10^{-19}$ m^2). However, Fig. 6a shows that the peak of C^* is always predicted at about 2 mm depth, whatever the value of K. These results contradict the assertion commonly found in literature without any justification, that the Cl concentration peak corresponds to the limit between the convection and diffusion zones.

Then, it appears that the calculated profiles are in good agreement with the measurements from a depth of 2 cm. Before 2 cm, Cl concentration are overestimated by simulations compared to measurements and the peak is actually measured at 1.7 cm. Exactly the same kind of discrepancies has been obtained by Achour (2018) comparing tidal cycles simulations and measurements. This may be explained by the so-called "skin effect" (Cai et al., 2020) consisting in alteration of material properties by mechanical damage or physicochemical leaching from the surface to a certain depth as well as in the washing effect of rains driving chloride out of this "skin". Note that these explanations are of a qualitative nature and still need further studies to be quantified experimentally.

Figure 6c shows $C_{Cl,tot}$ profiles obtained from simulation considering various values of K and a value of β of 1 (i.e., maximum effect of the partial saturation on Cl binding). It appears that at moderate to high values of K, the effect of considering a value of β of 1 is important and results in restraining the transport of Cl very significantly, literally stopping it for K of 10^{-19} m^2: this effect obviously lacks of some experimental observations. Therefore, it will be assumed the value of β remains low but not necessarily equal to zero: its possible range is presented in section 4.3.

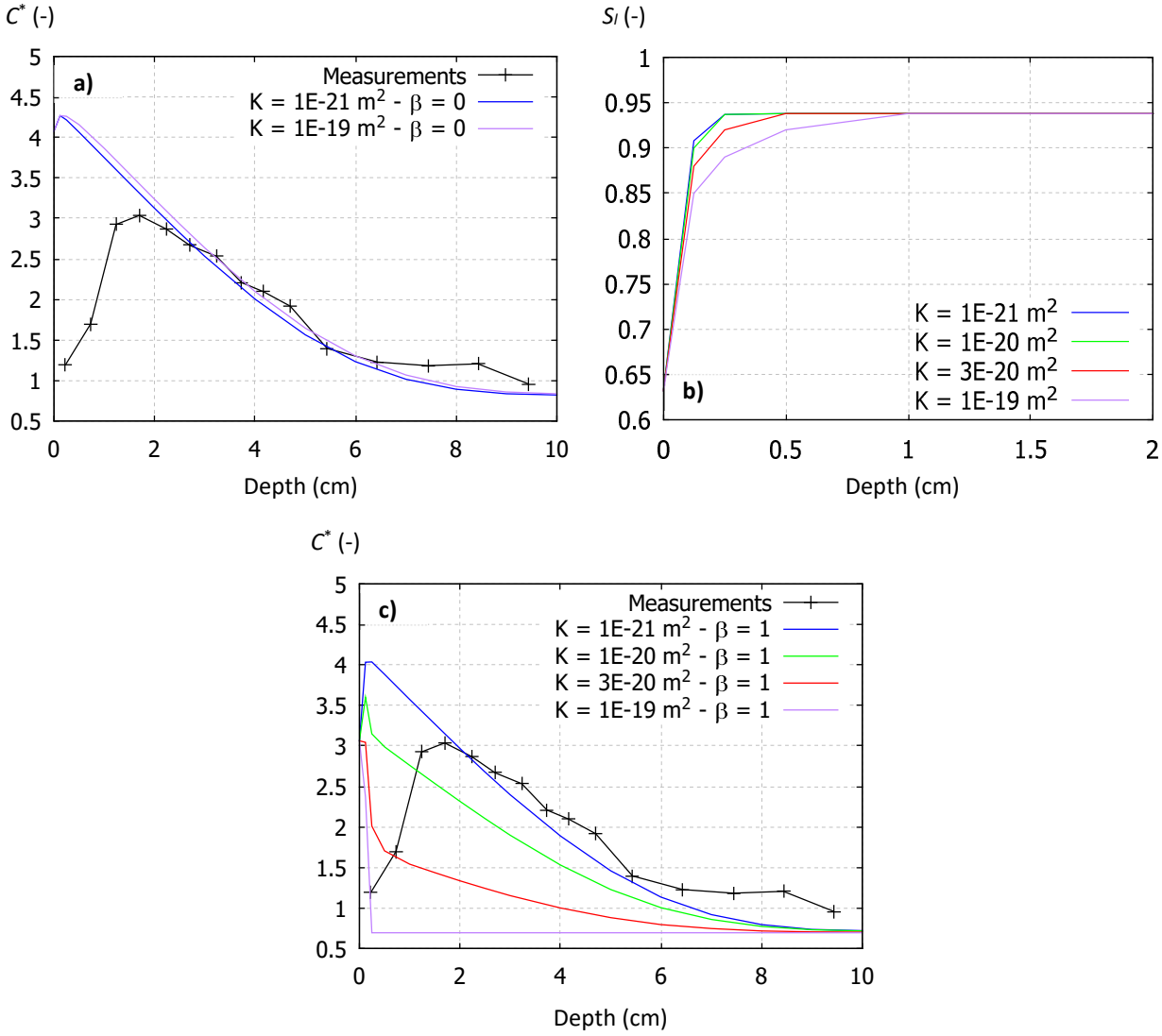

Figure 6: Concrete OPCC60, 28 years of exposition (a) profiles of C^* – measurements (Othmen et al., 2018), simulations with different values of K, (b) profiles of S_l predicted with different values of K, (c) profiles of C^* considering $\beta = 1$ and with different values of K.

4 Sensitivity analysis based on the simplified model

4.1 Morris method

First, n input parameters are considered: $X_1,\ldots, X_n$, each parameter X_i having a value in a given range $[X_{i,\min}, X_{i,\max}]$. From these parameters X_i, a simulation (or a function) leads to a response: $Y=Y(X_1, \ldots, X_n)$. The aim of a sensitivity analysis is to characterize the effect of a change of the value of X_i on the response Y. From the Morris method (Morris, 1991; Campolongo and Cariboni, 2007), every range $[X_{i,\min}, X_{i,\max}]$ is discretized in p levels. Let us consider initial random values: $X_{1,0},\ldots, X_{i,0},\ldots, X_{n0}$, for the input parameters (these values being in the given ranges and on one of their predefined levels) and the associated response: $Y(X_{1,0},\ldots, X_{i,0},\ldots, X_{n0})$. The next step consists in calculating the response: $Y(X_{1,0},\ldots, X_{i-1,0}, X_{i,0}+\delta_1\Delta X_i, X_{i+1,0},\ldots, X_{n0})$, where ΔX_i is $X_{i,\max}-X_{i,\min}$ and δ_1 allows a random change of level

(for instance, if $p = 4$, δ_1 is necessarily equal to one of these values: ±1/3, ±2/3 or ±1). The next step consists in calculating the response: $Y(X_{1,0},\ldots, X_{i-1,0}, X_{i,0}+\delta_1\Delta X_i, X_{i+1,0},\ldots,\ldots, X_{j-1,0}, X_{j,0}+\delta_2\Delta X_j, X_{j+1,0},, X_{n0})$. Thus, only one parameter is changed at a time, which finally consists in the generation of a trajectory of n+1 simulations. This operation is repeated r times, every time with different initial random values of the input parameters, which results in the generation of r trajectories. Thus, the total number of simulations to perform is $r(n+1)$.

Then, the analysis proposed by Morris consists in calculating the elementary effects ee_i by the following expression:

$$ee_i\left(X_i,\delta\right)=\frac{Y\left(X_1,\ldots,X_{i-1},X_i+\delta\cdot\Delta X_i,X_{i+1},\ldots,X_n\right)-Y\left(X_1,\ldots,X_n\right)}{\delta} \tag{20}$$

Finally, the following "sensitivity indexes" can be deduced:

- μ_i, the average of ee_i for input parameter X_i,

- μ_i^*, the average of $|ee_i|$,

- and $\sigma_{\mu i}$, the standard deviation of ee_i.

The values of these indexes can be analyzed in the following way (Andrianandraina et al., 2015):

- the higher the value of μ_i^* is, the higher on the output Y the effect of the input parameter X_i is,

- the sign of μ_i indicates the direction of the effect of X_i on Y, $\mu_i > 0$ suggests a positive correlation between X_i and Y and vice versa,

- $\sigma_i/\mu_i^* \leq 0.1$ indicates a linear relationship between X_i and Y,

- $0.1 < \sigma_i/\mu_i^* \leq 0.5$ indicates a monotonic relationship between X_i and Y,

- $\sigma_i/\mu_i^* > 0.5$ indicates a non-linear relationship between X_i and Y and / or interaction(s) with the other input parameters.

4.2 Analysis by an alternative quantitative method

Here, an alternate method of analysis (Reuge et al., 2020) will also be considered, consisting in calculating the elementary sensitivities es_i defined as follows:

$$es_i=\frac{\frac{\Delta Y}{\overline{Y}}\left(X_i,\delta\right)}{\frac{\Delta X}{\overline{X}}\left(X_i,\delta\right)}=\frac{\frac{Y\left(X_1,\ldots,X_{i-1},X_i+\delta\cdot\Delta X_i,X_{i+1},\ldots,X_n\right)-Y\left(X_1,\ldots,X_n\right)}{\frac{1}{2}\left[Y\left(X_1,\ldots,X_{i-1},X_i+\delta\cdot\Delta X_i,X_{i+1},\ldots,X_n\right)+Y\left(X_1,\ldots,X_n\right)\right]}}{\frac{\delta\cdot\Delta X_i}{\frac{1}{2}\left(2X_i+\delta\cdot\Delta X_i\right)}} \tag{21}$$

Finally, the following "sensitivity indexes" can be deduced:

- S_i, the average of es_i for input parameter X_i,

- S_i^*, the average of $|es_i|$,

- and σ_{Si}, the standard deviation of es_i.

Although the Morris method cannot really be considered as quantitative considering the moderate values of p and r, analysis performed from eq. (21) will bring indications of a more quantitative nature than eq. (20).

The values obtained for these indexes can be analyzed in exactly the same way as previously indicated.

4.3 Characterization of input parameters

Nine input parameters have been considered for this sensitivity analysis:

- seven parameters intrinsic to the material: φ, K, $D_{eff,0}$, λ, m, μ, and β,

- one parameter, S_{l0}, which is an initial hygric condition,

- and one parameter, C_{crit}, which is the threshold chloride concentration for initiation of corrosion.

The variation ranges chosen for the input parameters are given in Table 2.

Parameter	Min value	Max value
φ (-)	0.09	0.14
K (m^2)	10^{-21}	10^{-19}
$D_{eff,0}$ ($m^2.s^{-1}$)	2.10^{-13}	2.10^{-12}
λ (-)	4	8
m (-)	0.27	0.39
μ	3.5	6
β (-)	0	0.2
S_{l0} (-)	0.7	0.9
C_{crit} (wt%/b)	0.2	0.5

Table 2: Variation ranges of input parameters

For φ, K and $D_{eff,0}$, variation ranges have been chosen according to (Baroghel-Bouny et al., 2004). The range chosen for λ is centered on the value of 6 found in (Baroghel-Bouny et al., 2011). From the analysis performed in section 3.2.4, β is restrained to a relatively low maximum value of 0.2.

For sorption and binding parameters, three concretes studied in (Ben Fraj et al., 2012) have been considered: OPPC30 (ordinary concrete), OPCC60 (enhanced ordinary concrete) and BFS60 (high performance concrete with slag). From the investigations of Ben Fraj et al. (2012), sorption and binding measurements have been gathered in Figures 7a and 7b respectively. Thus, it has been possible to determine the following envelopes:

- for adsorption isotherm (VG model):

$$\begin{cases} S_l(Hr) = \left[1+\left(-\frac{\rho_w RT}{M_w}\cdot\frac{1}{5.6\cdot10^6}\ln(Hr)\right)^{\frac{1}{1-0.39}}\right]^{-0.39} \\ S_l(Hr) = \left[1+\left(-\frac{\rho_w RT}{M_w}\cdot\frac{1}{5.6\cdot10^6}\ln(Hr)\right)^{\frac{1}{1-0.27}}\right]^{-0.27} \end{cases} \quad (22,23)$$

- and for binding law (Freundlich model):

$$\begin{cases} C_{Cl,b}(c_{Cl,f}) = 3.5(c_{Cl,f})^{0.65} \\ C_{Cl,b}(c_{Cl,f}) = 6(c_{Cl,f})^{0.65} \end{cases} \quad (24,25)$$

Note that the envelopes have been chosen large enough compared to the measurement points. They provide the range for m and μ reported in Table 2, α and γ parameters being fixed at $5.6.10^6$ Pa and 0.65 respectively.

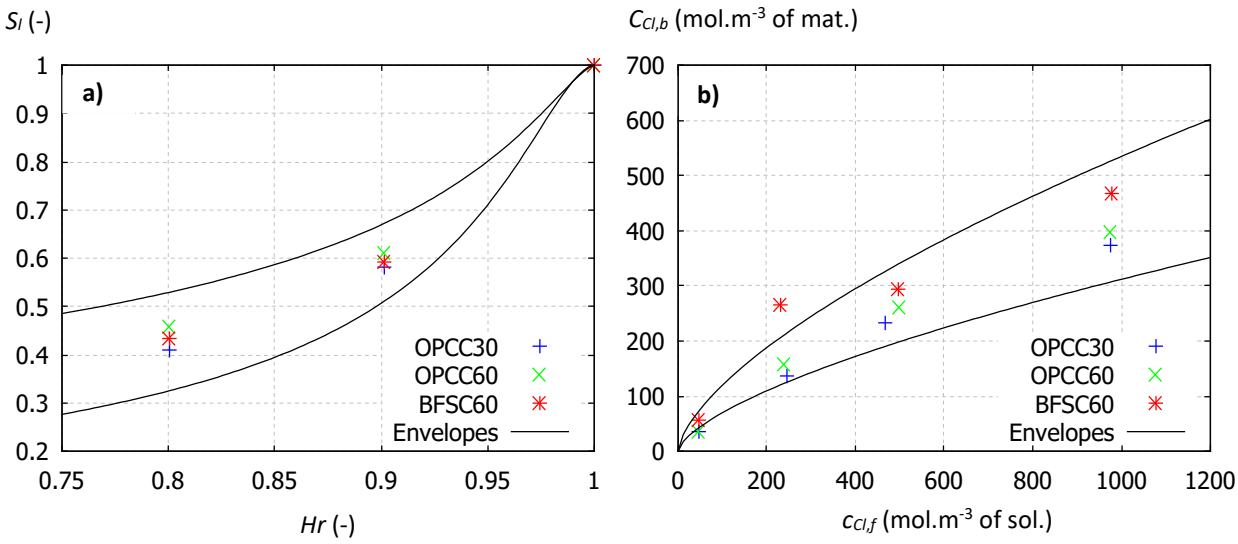

Figure 7: Concretes OPCC30, OPCC60 and BFSC60, (a) isotherms of adsorption, measurements (Ben Fraj, 2012) and envelops, (b) binding isotherms, measurements (Ben Fraj, 2012) and envelopes.

Regarding C_{crit} (wt%/binder), one can refer to the Beta distribution given in (Gelhen et al., 2015), with lowest bound at 0.2 and a mean of 0.6. In order to get reasonable calculation times, C_{crit} has been considered here in the range of 0.2 to 0.5. Note that from the on-site data provided by Angst et al. (2009), 0.5 appears to be a very common value for C_{crit}. More in-depth study could take into account some parameters having an effect on C_{crit} such as O_2 diffusion rate which is promoted in unsaturated conditions (Angst et al., 2009; Melchers, 2009; Ohno et al, 2022), steel potential or pH of the pore solution, etc. (Angst et al., 2009) but this would add level of complexity difficult to handle in the whole approach. Note that the binder quantity C_b has been considered equal to 350 kg.m^{-3} (Ben Fraj

et al., 2012) which is in agreement with the standard for concrete exposed to tidal conditions (EN 206-1, 2004).

4.4 Simulated scenario

Ten trajectories have been generated by the Morris method with a discretization in p = 4 levels for each of the nine input parameters. From (Campolongo and Cariboni, 2007; Franczyk, 2019), this is statistically sufficient to get reliable results with this method. Thus, it led to a total of 100 parameter sets.

The 100 simulations have been performed using the physicochemical model described in sections 2.1 and 2.2. A depth L of 10 cm was still considered. Tidal cycles boundary conditions have been given in section 3.2.1. In future studies, it will be interesting to characterize the effects of modifying the tidal conditions but in the present study, the aim is mostly to characterize the effect of the intrinsic material parameters.

The response parameter has been defined as the time t_{crit} necessary to obtain the concentration C_{crit} at 3 cm depth inside the material. Simulations were stopped at t_{crit} which were in the range of 3 years to 1375 years and therefore involving very long simulations for some sets of input parameters. Regarding the depth at which C_{crit} has been studied (i.e., 3 cm), it would have been more relevant to choose it at 5 cm regarding the standards of the concretes in marine environments but it would have led to unreasonably long simulations for some sets of input parameters. Transposing the results obtained at 3 cm to results that would have been obtained at deeper depths is a delicate question. But since the material is assumed homogeneous in space and time and that the chloride transport mechanism remains dominated by diffusion at such depths, it is reasonable to expect that the order of influence of the different input parameters would remain the same. Note that the 100 simulations have required a total of about 15 000 h CPU to be completed.

4.5 Results

Results obtained by the analysis of Morris are presented in Table 3. Input parameters have been sorted according to the importance of their effects which are determined by the values of μ_i^*. According to this analysis, 4 parameters can be considered as very influential: $D_{eff,0}$, C_{crit}, β and λ; 2 parameters as moderately influential: K and m; and 3 parameters as weakly influential: Sl_0, μ and φ. The signs of μ_i^*/μ_i show that an increase of $D_{eff,0}$ results in a decrease of t_{crit} (negative sign) whereas an increase of C_{crit} results in an increase of t_{crit} (positive sign). According to the values of the ratios $\sigma_{\mu i}/\mu_i^*$ shown in Table 3, none of the studied parameters has a linear or monotonic effect on t_{crit}.

Table 4 shows the results with the quantitative method presented in section 4.2. Input parameters have been sorted according to the importance of their effect which is determined by the value of S_i^*. According to this analysis, 3 parameters can be considered as very influential: C_{crit}, $D_{eff,0}$ and λ; 3 parameters as moderately influential: m, μ and S_{l0}; and 3 parameters as weakly influential: β, K and φ. According to the values of the ratio σ_{Si}/S_i^*, the effects of C_{crit} and $D_{eff,0}$ can be considered as monotonic and linear respectively whereas the effects of the other parameters are non-linear and / or some significant interactions occur with some other input parameters.

As explained in section 4.1 and further detailed in section 5, the results obtained by this quantitative analysis have a more practical significance than those obtained by the Morris analysis; thus, the quantitative method will be retained for the further analysis in this study.

It must be emphasized that despite the input parameter *K* has a low effect on t_{crit}, this does not mean that the Darcy's flow has also a low global effect, this means that in the considered range of *K*, the effect of the Darcy's flow varies slightly.

Comparing these results of parameters sensitivities on t_{crit} with those of Kiesse et al. (2020) obtained by using Sobol and Morris methods on the basis of the 2nd law of Fick, the agreement is good regarding the great importance of D_{eff} and the moderate or low importance of the Cl binding parameter (μ in this study, slope of the binding isotherm in their study). However, a great importance of C_{crit} is also predicted here whereas their results show a significant effect of this parameter but moderate compared to D_{eff}.

Considering the quantitative method, if variations of a given input parameter lead to S_i^*/S_i close to ±1, the following estimation can be deduced from eq. (21):

$$Y\left(X_1,...,X_{i-1},X_i+\delta\cdot\Delta X_i,X_{i+1},...,X_n\right)=\left[\frac{2+\frac{\Delta X}{\overline{X}}\left(X_i,\delta\right)\cdot S_i}{2-\frac{\Delta X}{\overline{X}}\left(X_i,\delta\right)\cdot S_i}\right]Y\left(X_1,...,X_n\right) \quad (26)$$

Input Parameters	μ_i^*	μ_i^*/μ_i	$\sigma_{\mu i}/\mu_i^*$
$D_{eff,0}$	433.0	-1	0.8
C_{crit}	209.5	1	1.3
β	122.7	5	1.9
λ	90.8	-3.3	2.2
K	64.0	-3.8	1.8
m	63.9	1	2.3
S_{l0}	24.1	1	1.8
μ	15.9	-2.5	1.8
φ	4.2	-1.4	1.3

Table 3: Statistical analysis by the Morris method applied on input parameters

Input Parameters	S_i^*	S_i^*/S_i	σ_{Si}/S_i^*
C_{crit}	1.05	1	0.30
$D_{eff,0}$	0.99	-1	0.06
λ	0.62	12.4	1.56
m	0.37	1	1.05
μ	0.26	8.7	1.27
S_{l0}	0.22	1	1.05
β	0.15	3	1.60
K	0.08	2	1.13
φ	0.08	-2.7	1.00

Table 4: Statistical analysis by the quantitative method applied on input parameters

The variations of $D_{eff,0}$ lead to S_i^*/S_i of -1, so this relation can be applied. For instance, if a simulation 1 considering $D_{eff,0}$ of 2.10^{-12} $m^2.s^{-1}$ leads to a time $t_{crit,1}$, the time $t_{crit,2}$ of a simulation 2 considering $D_{eff,0}$ of 2.10^{-13} $m^2.s^{-1}$ can be estimated by:

$$t_{crit,2} = \left[\frac{2+(-1.63)(-0.99)}{2-(-1.63)(-0.99)}\right] t_{crit,1} \approx 10 \cdot t_{crit,1} \quad (27)$$

Results of the simulations are in reasonably good agreement with this estimation. Therefore, eq. (26) has a quite interesting practical application in predicting the responses.

5 Analysis and discussion

5.1 Comparison of simulation results with various data of the literature

When an engineering model based on the Fick's 2nd law is used, it is supposed to be used from the limit of the convection / diffusion zones at a certain depth L_c and for a given total chloride concentration $C_{Cl,tot}$ at this depth. However, this depth and its corresponding Cl content are a priori unknown, they can only be estimated by statistical distributions such as the ones provided by Gelhen et al. (2015), presumably based on a significant number of experimental data. Simulations performed in the frame of this SA have allowed to determine their values at t_{crit} so that it seems interesting to compare them with the statistical distributions provided by the fib model code (Gelhen et al., 2015). From the simulations, the convection depths L_c have been determined at the position where S_l was equal to $0.99 \cdot S_l(x = L = 10$ cm). Note that for 29 of the 100 simulations, the limit of the convection / diffusion zones was not yet stabilized at t_{crit}, therefore the associated distributions presented below take only into account the 71 other usable simulations.

Figure 8a shows the probability density function of L_c given by the fib model code (XS3 exposure class) represented by a Beta distribution (Gelhen et al., 2015), its mean being at L_c of 10 mm. The distribution of L_c provided by the 71 simulations has been added to this Figure, its mean being at L_c of 5 mm: it can clearly be seen that the simulations underpredict L_c compared to the fib model code distribution. The discrepancy is certainly linked with the aforementioned "skin effect".

Figure 8b shows the probability density functions of $C_{Cl,tot}$ at L_c given by the fib model code (XS3 exposure class) represented by two lognormal distributions corresponding to the most favorable / unfavorable scenarios (Gelhen et al., 2015) with means at 2 and 4 %wt/binder respectively. The distribution provided by the 71 simulations has been added to Fig. 8b, leading to a mean at $C_{Cl,tot}$ of 3.3 %wt/binder which is consistent with the fib model code distributions. Note that the range of admissible $C_{Cl,tot}$ provided by these fib model code distributions exceed the one obtained from the simulations.

From the work of Carcassès et al. (2021), Figure 9a shows L_c as a function of φ for measurements performed during the BHP 2000 campaign (Baroguel-Bouny et al., 2013) and from other experimental data found in literature (Lindvall, 2003; Moradlo et al., 2018; Wang et al., 2018; Gao et al., 2019; Mai-Nuh et al., 2019a). Despite the significant dispersion of the points, Carcassès et al. (2021) have proposed to express L_c as a function of φ by a power law (Fig. 9a).

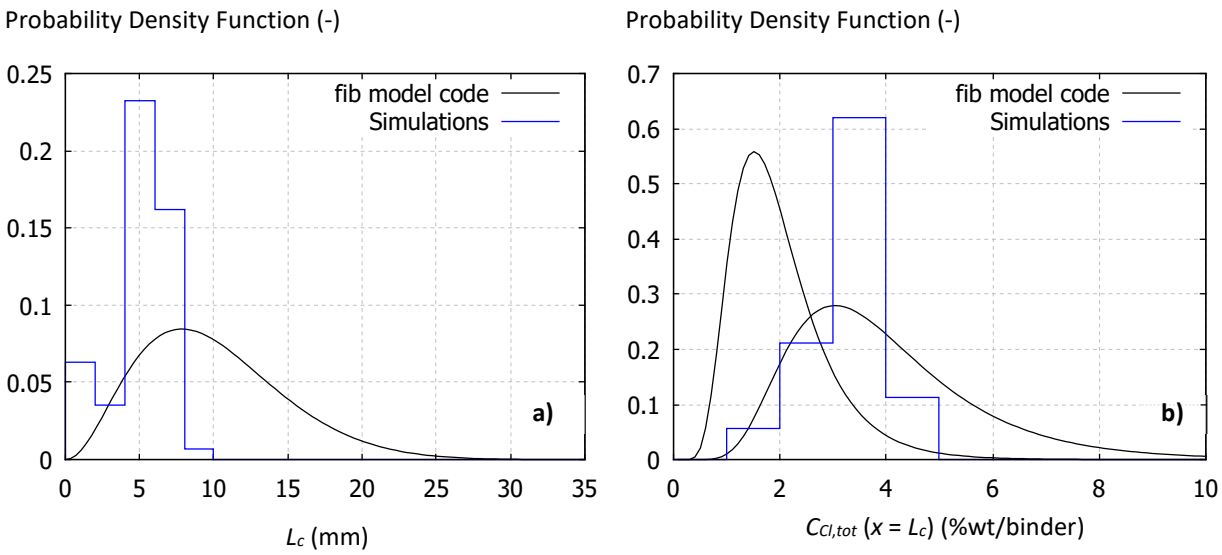

Figure 8: Probability density functions, (a) for L_c from fib model code (Gelhen et al., 2015) and from simulations, (b) for $C_{Cl,tot}$ at L_c from fib model code (Gelhen et al., 2015) and from simulations.

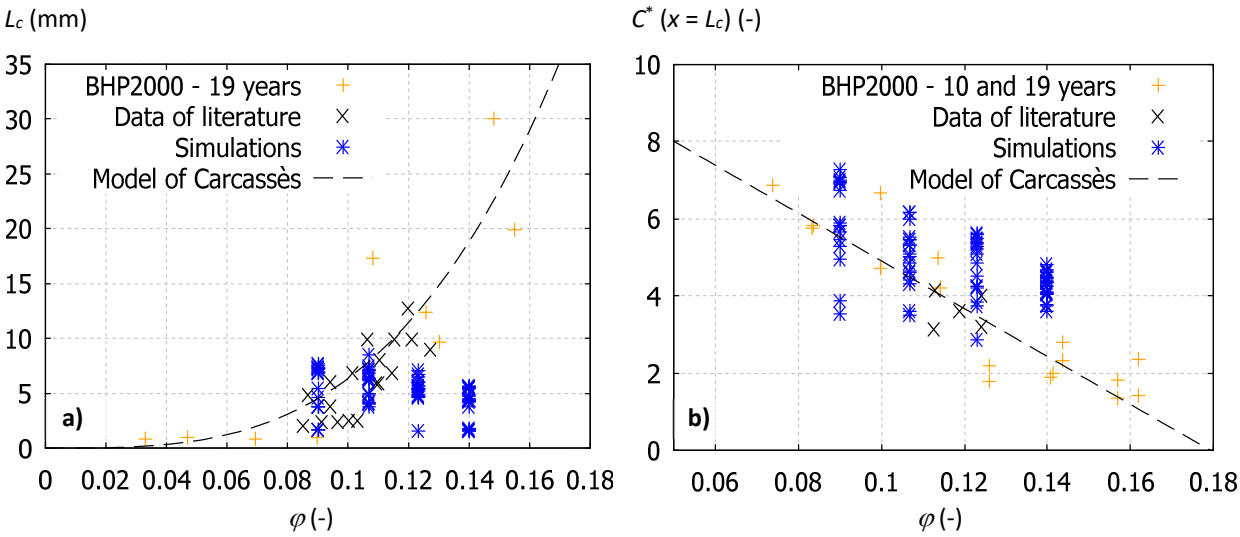

Figure 9: (a) L_c as a function of φ from measurements and from simulations, (b) C^* at L_c as a function of φ from measurements and from simulations.

The results of the 71 simulations have been added in Fig. 9a. As already seen, simulations tend to underestimate L_c compared to measurements. The simulations points obtained at high porosities ($\varphi \geq 0.12$) differ with the experimental points or the empirical law of Carcassès et al. (2021). That said, note that the experimental points are very few in the range of such high porosities (i.e., [0.12, 0.16]). To explain these differences, one can be tempted to deduce that so high porosities involve intrinsic permeabilities K greater than the upper bound considered in this SA (i.e., 10^{-19} m^2). However, this upper bound is based on laboratory measurements (Baroghel-Bouny et al. 2004). Again, the role of a "skin effect" has to be mentioned. As seen above, many phenomena can lead to the appearance of

this "skin effect", such as surface cracks (Wang et al., 2016). Their quantification is a vast field of future investigations and is beyond the scope of this study. In any event, data obtained from the simulations do not follow the trend of the simple power law provided by Carcassès et al. (2021), suggesting that φ is not the only input parameter that play a role in the value of L_c.

Still from the work of Carcassès et al. (2021), Figure 10b shows C^* at L_c as a function of φ for measurements performed during the BHP 2000 campaign (Baroguel-Bouny et al., 2013) and from other experimental data found in literature (Mai-Nuh et al., 2019a; Mai-Nuh et al., 2019b). Carcassès et al. (2021) have deduced a linear relationship between C^* at L_c and φ.

The results of the 71 simulations have been added in Fig. 9b. They are in agreement with the experimental data but their dispersion is very important. Note the dispersion of experimental data are also quite important. This suggests that φ is not the only input parameter controlling the value of C^* at L_c.

5.2 Physically informed analysis and guidelines in using engineering models

As explained above, 71 simulations performed in the frame of this SA have allowed determining L_c and $C_{Cl,tot}$ at L_c at t_{crit}, which are in reasonable agreement with experimental data, excepted at high porosities regarding L_c. Thus, it seems interesting to quantify the effects of the input parameters on them.

5.2.1 Estimation of L_c

According to the different simulations, L_c varies from 1.5 mm to 8.5 mm. Results of the SA are reported in Table 5. According to these results, 3 parameters can be considered as very influential: φ, m and K, and 2 parameters are moderately influential: S_{l0} and λ. The other parameters are very weakly or not influential at all.

Input Parameters	S_i^*	S_i^* / S_i	σ_{Si} / S_i^*
φ	0.77	-1	1.42
m	0.69	1	1.72
K	0.53	1	0.30
S_{l0}	0.38	-1	3.03
λ	0.28	1	2.21
β	0.05	1	2.40
C_{crit}	0	-	-
$D_{eff,0}$	0	-	-
μ	0	-	-

Table 5: Sensitivity analysis on L_c, statistical results

The aim is now to find an analytical relation expressing L_c as a function of the influent input parameters. From Darcy's law (1), an estimate of the characteristic distance Δx over which the liquid can be transported in a time Δt is derived as follows:

$$\left(\Delta x\right)^2 = \Delta t.Kk_{r,l}\eta_l^{-1}\Delta P_c \tag{28}$$

Replacing ΔP_c by αP_c, one gets:

$$\left(\Delta x\right)^2 = \alpha\Delta t.Kk_{r,l}\eta_l^{-1}P_c \tag{29}$$

α being actually relatively constant and L_c stabilizing from a given Δt, by using eqs. (4) and (5), one gets:

$$L_c = \sqrt{a_1 K S_l^{1/2}\left[1-\left(1-S_l^{1/m}\right)^m\right]\left(S_l^{-1/m}-1\right)^{1-m}} \tag{30}$$

where a_1 and S_l are adjustable parameters. Performing the adjustment with respect to the values of L_c deduced from the simulations (and the associated input parameters K and m), the following values are obtained: $a_1 = 8.05.10^{21}$ and $S_l = 0.95$, with a correlation coefficient r of 0.942 (note that the adjustment value obtained for S_l corresponds with its value predicted by the simulations in the diffusion zone).

The input parameter φ does not appear in this relation, however it is a quite influent parameter from the analysis of Table 5. It is introduced in eq. (30) as follows:

$$L_c = \varphi^{b_1}\sqrt{a_1 K S_l^{1/2}\left[1-\left(1-S_l^{1/m}\right)^m\right]\left(S_l^{-1/m}-1\right)^{1-m}} \tag{31}$$

where b_1 is an adjustable parameter. Performing the adjustment again, the following values are obtained: $a_1 = 9.09.10^{20}$, $b_1 = -0.5$ and $S_l = 0.95$, with a correlation coefficient r of 0.973. This leads to a mean discrepancy of L_c estimated / simulated of ±0.27 mm, which is quite small. Values of L_c estimated / simulated are compared in Figure 10a.

5.2.2 Estimation of $C_{Cl,tot}$ at L_c

It is also interesting to perform the SA on $\overline{C}_{Cl,tot}\left(x=L_c\right)/\overline{C}_{Cl,tot}\left(x=0\right)$ where $\overline{C}_{Cl,tot}\left(x=0\right)$ is a known mean boundary conditions, it can be very well estimated by the following relation:

$$\begin{aligned}\overline{C}_{Cl,tot}\left(x=0\right) &= \overline{C}_{Cl,f}\left(x=0\right)+\overline{C}_{Cl,b}\left(x=0\right)\\ &= \varphi\frac{1}{2}\left(S_{l,\min}+S_{l,\max}\right)c_{Cl,sea}+\mu\frac{1}{2}\left(S_{l,\min}^{\beta\gamma}+S_{l,\max}^{\beta\gamma}\right)c_{Cl,sea}^{\gamma}\end{aligned} \tag{32}$$

where $S_{l,min}$ and $S_{l,max}$ are given by the VG model for RH of 80% and 99.9% respectively. Thus, through this relation, $\overline{C}_{Cl,tot}\left(x=0\right)$ integrates a dependence over the parameters μ, m, φ, and β.

The SA performed on $\overline{C}_{Cl,tot}\left(x=L_c\right)/\overline{C}_{Cl,tot}\left(x=0\right)$ at t_{crit} is given in Table 6. It appears that no parameter can be considered as very influential and 2 parameters as moderately influential: m and φ.

Actually, most of the influence of μ and part of the influences of m and φ are taken into account through the denominator $\overline{C}_{Cl,tot}\left(x=0\right)$.

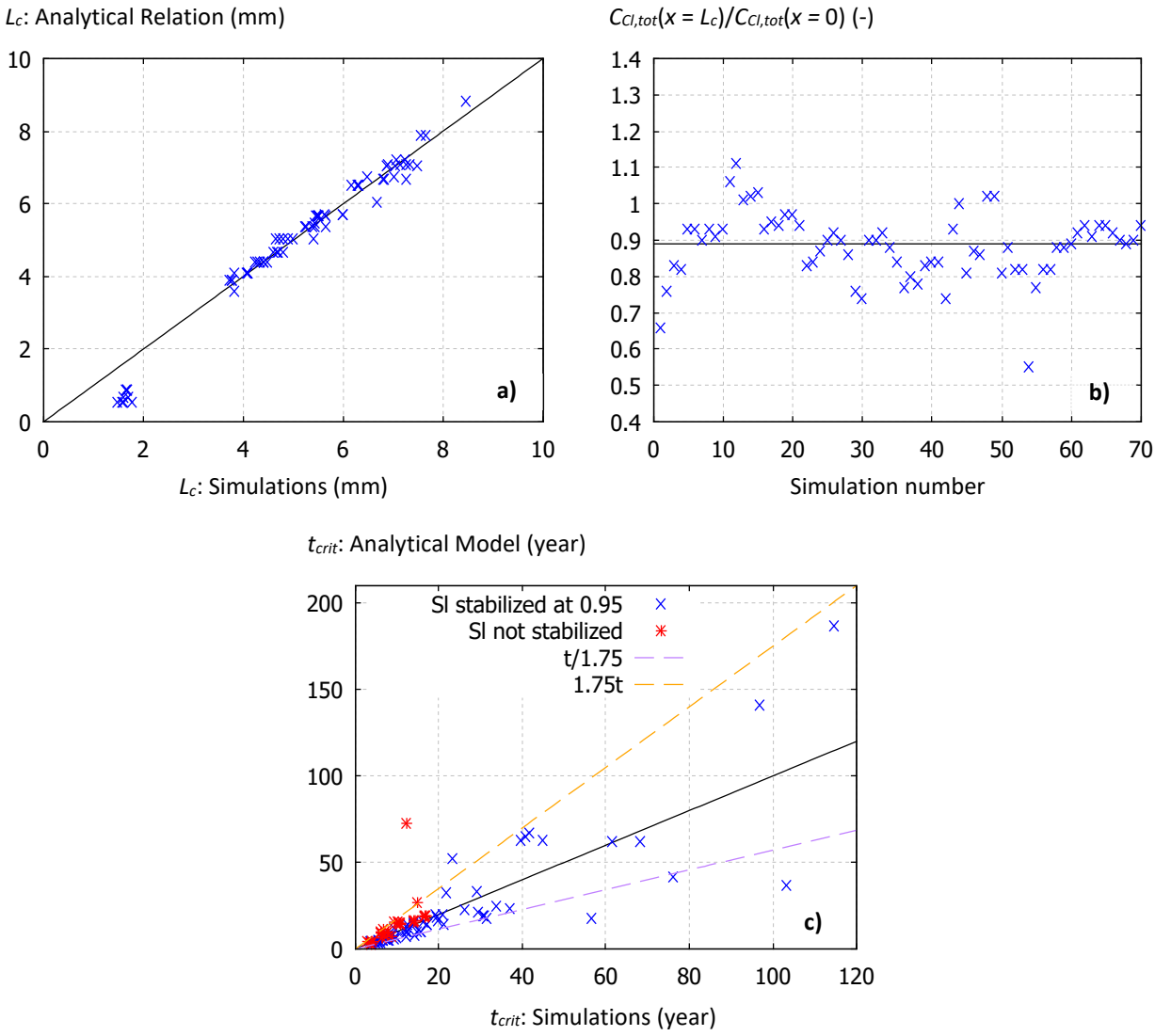

Figure 10: (a) L_c obtained from analytical relation (34) vs L_c obtained from simulations, (b) distribution of $C_{Cl,tot}(x = L_c)/C_{Cl,tot}(x = 0)$ obtained from simulations around 0.89, (c) t_{crit} obtained from analytical model (33,34,35,36) (black line) vs t_{crit} obtained from simulations.

Broadly, by averaging the results of the 71 simulations, $\overline{C}_{Cl,tot}\left(x = L_c\right)/\overline{C}_{Cl,tot}\left(x = 0\right)$ can be estimated to 0.89 with a standard deviation of only 0.09. Dispersion of the points around 0.89 is shown in Figure 10b.

Input Parameters	S_i^*	S_i^* / S_i	σ_{Si} / S_i^*
m	0.33	-1	0.82
φ	0.27	1	1.22
λ	0.13	-1	1.38
β	0.12	-1.5	1.25
μ	0.12	-1	0.42
K	0.11	-1	0.82
S_{l0}	0.07	1.2	2.86
C_{crit}	0.07	1	0.71
$D_{eff,0}$	0.05	1.25	1.00

Table 6: Sensitivity analysis on $\overline{C}_{Cl,tot}\left(x=L_c\right)/\overline{C}_{Cl,tot}\left(x=0\right)$ at t_{crit}, statistical results

5.2.3 Estimation of t_{crit}

The two previous estimates are highly interesting since they can be used in engineering models based on the Fick's 2nd law. According to this law, considering a depth of 3 cm, t_{crit} can be estimated by the following expression (Kiesse et al., 2020):

$$t_{crit} = \frac{1}{4D_{app}}\left[\left(0.03 - L_c\right) \Big/ \operatorname{erfc}^{-1}\left(\frac{C_b C_{crit}}{\overline{C}_{Cl,tot}\left(x=L_c\right)}\right)\right]^2 \tag{33}$$

And using the previously determined relations:

$$\begin{cases} L_c = \sqrt{9.09\cdot 10^{20}\,\dfrac{K}{\varphi}\,0.95^{1/2}\left[1-\left(1-0.95^{1/m}\right)^m\right]\left(0.95^{-1/m}-1\right)^{1-m}} \\ \overline{C}_{Cl,tot}\left(x=L_c\right) = 0.89\left[\dfrac{1}{2}\varphi\left(S_{l,\min}+S_{l,\max}\right)c_{Cl,sea} + \dfrac{1}{2}\mu\left(S_{l,\min}^{\beta\gamma}+S_{l,\max}^{\beta\gamma}\right)c_{Cl,sea}^{\gamma}\right] \\ D_{app} = \dfrac{0.95^{\lambda}\,D_{eff,0}}{\varphi+0.46} \end{cases} \tag{34,35,36}$$

where D_{app} is the apparent Cl ions diffusivity and the value of 0.46 corresponds to the mean slope of the binding isotherms assumed as linear, considering all points in Fig. 7b (i.e., linear regression). In the diffusion zone, simulations predict a constant value of S_l stabilized at a value of about 0.95, therefore, from relation (10), D_{eff} can be considered as equal to $D_{eff,0}(0.95)^{\lambda}$.

It should be emphasized that while the engineering approach given by the fib model code (Gelhen et al., 2015) restricts to provide probability density functions for L_c and $\overline{C}_{Cl,tot}\left(x=L_c\right)$, analytical relations provided by Eqs. (34, 35 and 36) allow to estimate these data as functions of the input parameters.

Values of t_{crit} estimated / simulated are compared in Figure 10c. It appears that the average discrepancy of t_{crit} obtained by relations (33, 34, 35 and 36) with regard to the 71 simulations is of ±27% and is centered on -10%. Thus, despite the good estimations of L_c and $\overline{C}_{Cl,tot}\left(x=L_c\right)$ provided

by the analytical relations (33) and (34), there are still some significant discrepancies between calculated and estimated t_{crit}: this can be explained by the dynamic nature of the transport phenomena (in simulations and of course in reality) compared to the static and averaged nature of the analytical approach. Thus, static engineering approaches cannot reach the same degree of precision as dynamic simulations based on a physicochemical description of the phenomena. Values of t_{crit} estimated / simulated for the remaining 29 sets of input parameters have been added in Fig. 10c, the average discrepancy is of ±45%. Globally, in Figure 10c, 95% of the points are spread between the two dashed lines $t/1.75$ and $1.75t$.

Thus, thanks to the SA and from the results of the physico-chemical model, interesting and physically informed guidelines have been deduced in the form of analytical relations, allowing to obtain estimations of t_{crit} via the Fick's 2nd law to a certain degree of confidence.

6 Conclusion

In order to predict chloride ingress into concrete, a physicochemical approach based on some clearly stated assumptions has been proposed. Some further simplifications have been checked to be pertinent for tidal conditions: ignoring the kinetics of Cl physisorption, considering the sorption isotherms and liquid relative permeabilities of adsorption only. It is valuable for restricting the number of input parameters needed for a SA.

Simulations have been compared to on-site measurements after long exposure and revealed to properly predict the chloride concentration in the depth of the exposed concrete despite the lack of representation of a so called "skin effect".

Sensitivity analysis has been carried out and involved 100 simulations. Their results were interpreted according to two methods: Morris method and an alternate one of a more quantitative significance. From the results, the following conclusions can be drawn:

- According to both analysis methods, the parameters playing the most critical role on the critical time of initiation of corrosion are the critical concentration and the effective chloride diffusivity parameters. Moisture sorption and chloride binding parameters have a more moderate effect. Thus, it provides valuable indications on properties that must be characterized accurately.

- Analysis by the quantitative method has shown that the depth of the convection zone is mainly determined by the material porosity, its sorption capacity and its permeability.

- The total chloride concentration at the limit of convection / diffusion zones is mainly determined by the material binding and sorption capacities and its porosity.

Results from the simulations performed for the SA have been compared to the distributions provided by the fib model code (XS3 exposure class) and to experimental data provided in literature in terms of convection depth and average total chloride concentration at this depth:

- The agreement is good for the total chloride concentration but the simulations do not accurately predict the peak position as experimental results found in literature: this is certainly linked with the aforementioned "skin effect".

- Analytical relations expressing convection depth and average total chloride concentration at this depth as functions of the influent input parameters have been developed.

- They represent physically informed guidelines that are very useful performing estimations using a model based on the Fick's 2nd law.

- Critical times of initiation of corrosion has been estimated analytically and the average discrepancy with the simulations has revealed to be of ±27%.

Acknowledgements

Région Pays de La Loire (France) is gratefully acknowledged for supporting this study which was developed in the frame of the DEMCOM Project (grant ANR-20-CE22-0008-03) funded by the French National Research Agency. The writing of this article has been achieved in the frame of the project B2FE, granted by WEAMEC with support of Région Pays de La Loire, FEDER, CARENE and Nantes Métropole (France).

References

Achour, M., 2018. Modélisation du couplage carbonatation – chlorures et étude multiéchelle de l'influence des granulats sur la diffusivité dans les bétons. Ph.D. Thesis. Ecole Centrale de Nantes. France.

Achour, M., Amiri, O., Bignonnet, F., Roziere, E., 2019. Influence of carbonation on ionic transport in unsaturated concrete: evolution of porosity and prediction of service life. Eur. J. Environ. Civ. En. 23, 593–608. https://doi.org/10.1080/19648189.2018.1455609.

Al-Rabiah, A.R., Rasheeduzzafar, Baggott, R., 1990. Durability Requirements for Reinforced Concrete Construction in Aggressive Marine Environments. Mar. Struct. 3, 285–300. https://doi.org/10.1016/0951-8339(90)90013-H.

Andrianandraina, Ventura, A., Kiesse, T.S., Cazacliu, B., Idir, R., van der Werf, H.M.G., 2015. Sensitivity Analysis of Environmental Process Modeling in a Life Cycle Context: A Case Study of Hemp Crop Production. J. Ind. Ecol. 19, 978–993. https://doi.org/10.1111/jiec.12228.

Angst, U., Elsener, B., Larsen, C.K., Vennesland, O., 2009. Critical chloride content in reinforced concrete – A review. Cement Concrete Res. 39, 1122–1138. https://doi.org/10.1016/j.cemconres.2009.08.006.

Atkins, P.W., 1985. Physical Chemistry. 3rd ed. Oxford University Press.

Bamforth, P.B., 1987. The relationship between permeability coefficients for concrete obtained using liquid and gas. Mag. Concrete Res. 39, 3–11. https://doi.org/10.1680/macr.1987.39.138.3.

Bao, J., Zheng, R., Wei, J., Zhang, P., Xue, S., Liu, Z., 2022. Numerical and experimental investigation of coupled capillary suction and chloride penetration in unsaturated concrete under cyclic drying-wetting condition. J. Build. Eng. 51, In press. https://doi.org/10.1016/j.jobe.2022.104273.

Baroghel-Bouny, V., Andrade, C., Castellote, M., Brazillier, D., Costaz, J.L., Couty, R., et al., 2004. Concrete design for structures with predefined service life – Durability control with respect to reinforcement corrosion and alkali–silica reaction, state-of-the-art and guide for the implementation of a performance-type and predictive approach based upon durability indicators. English version of Documents Scientifiques et Techniques de l'AFGC (Civil Engineering French Association).

Baroghel-Bouny, V., Thiery, M., Wang, X., 2011. Modelling of isothermal coupled moisture–ion transport in cementitious materials. Cement Concrete Res. 41, 828–841. https://doi.org/10.1016/j.cemconres.2011.04.001.

Baroghel-Bouny, V., Dierkens, M., Wang, X., Soive, A., Saillio, M., Thiery, M., Thauvin, B., 2013. Ageing and durability of concrete in lab and in field conditions: investigation of chloride penetration. J. Sustain. Cem.-Based Mater. 2, 67–110. https://doi.org/10.1080/21650373.2013.797938.

Ben Fraj, A., Bonnet, S., Khelidj, A., 2012. New approach for coupled chloride/moisture transport in non-saturated concrete with and without slag. Constr. Build. Mater. 35, 761–771. https://doi.org/10.1016/j.conbuildmat.2012.04.106.

Boddy, A., Bentz, E., Thomas, M.D.A., Hooton, R.D., 1999. An overview and sensitivity study of a multimechanistic chloride transport model. . Cement Concrete Res. 29, 827–837. https://doi.org/10.1016/S0008-8846(99)00045-9.

Bonnet, S., Perrin, B., 1999. Chloride influence on equilibrium properties of mortars. In French in Mater. Struct., 492-499.

Bonnet, S., Balayssac, J.P., 2018. Combination of the Wenner resistivimeter and Torrent permeameter methods for assessing carbonation depth and saturation level of concrete. Constr. Build. Mater. 188, 1149–1165. https://doi.org/10.1016/j.conbuildmat.2018.07.151.

Bonnet, S., Ventura, A., Villain, G., Cremona, C., Bignonnet, F., Palma Lopes, S. et al., 2022. DEMCOM Project: Durable and Environmental design of Monitored Concrete structures in Marine environment. French National Conference on Wind turbines, Paris, France.

Buchwald, A., 2000. Determination of the ion diffusion coefficient in moisture and salt loaded masonry materials by impedance spectroscopy. Proc. 3rd Int. Ph.D. Symp., Vienna, Austria, vol. 2, p 475–482.

Cai, R., Hu, Y., Yu, M., Liao, W., Yang, L., Kumar, A. et al., 2020. Skin effect of chloride ingress in marine concrete: A review on the convection zone. Constr. Build. Mater. 262, In press. https://doi.org/10.1016/j.conbuildmat.2020.120566.

Campolongo, F., Cariboni, J., 2007. Sensitivity analysis: how to detect important factors in large models. European Commission, Joint Research Centre, Ispra (VA), Italy. https://publications.jrc.ec.europa.eu/repository/bitstream/JRC37120/7120%20-%20eur_report_handbook_2.pdf

Carcassès, M., Chalhoub, C., El Farissi, A., Turcry, P., Mai-Thu, J., Ait-Alaiwa, A., et al., 2021. "MODEVIE" project: proposal of new service-life model. fib2020 Symposium Conference, Shanghai, China.

Chen, D., Ni, P., Li, Y., Mei, G., Xiao, L., Feng, J., 2022. An analytical solution of a finite domain convection-diffusion model for chloride intrusion into RC seawall. Appl. Ocean Res. 118, In press. https://doi.org/10.1016/j.apor.2021.103002.

EN 206-1 Concrete, 2004. Part 1: Specification, performances, production and conformity.

EN 1992-1-1 Eurocode 2, 2005. Design of concrete structure – Part 1.1 General rules and rules for buildings. European Standard Organization.

Francy, O., Francois, R., 1998a. Measuring chloride diffusion coefficients from non-steady State diffusion tests. Cement Concrete Res. 28, 947–953. https://doi.org/10.1016/S0008-8846(98)00070-2.

Francy, O., 1998b. Modélisation de la pénétration des ions chlorures dans les mortiers partiellement saturés en eau. Ph.D. Thesis. INSA, Toulouse, France.

Franczyk, A., 2019. Using the Morris sensitivity analysis method to assess the importance of input variables on time-reversal imaging of seismic sources. Acta Geophys. 67, 1525–1533. https://doi.org/10.1007/s11600-019-00356-5.

Gao, Y., Zheng, Y., Zhang, J., Wang, J., Zhou, X., Zhang, Y., 2019. Randomness of critical chloride concentration of reinforcement corrosion in reinforced concrete flexural members in a tidal environment. Ocean Eng. 172, 330–341. https://doi.org/10.1016/j.oceaneng.2018.11.038.

Gelhen, C., Bartholomew, M., Edvardsen, C., Ferreira, M., Von Greve-Dierfeld, S., Gulikers, J. et al., 2015. Fib 76 bulletin. Technical report. Fédération internationale du béton (fib). ISSN 1562-3610. ISBN 978-2-88394-116-8. https://www.afgc.asso.fr/app/uploads/2010/07/fib_Bulletin_76.pdf.

Kameche, Z.A., Ghomari, F., Choinska, M., Khelidj, A., 2014. Assessment of liquid water and gas permeabilities of partially saturated ordinary concrete. Constr. Build. Mater. 65, 551-565. https://doi.org/10.1016/j.conbuildmat.2014.04.137.

Kast, W., Hohenthanner, C.R., 2000. Mass transfer within the gas-phase of porous media. Int. J. Heat Mass Tran. 43, 807–823. https://doi.org/10.1016/S0017-9310(99)00158-1.

Kiesse, T.S., Bonnet, S., Amiri, O., Ventura, A., 2020. Analysis of corrosion risk due to chloride diffusion for concrete structures in marine environment. Mar. Struct. 73, In press. https://doi.org/10.1016/j.oceaneng.2016.09.044.

Kirkpatrick, T.J., Weyers, R.E., Anderson-Cooka, C.M., Sprinkel, M.M., 2002. Probabilistic model for the chloride-induced corrosion service life of bridge decks. Cement Concrete Res. 32, 1943–1960. https://doi.org/10.1016/S0008-8846(02)00905-5.

Li, D., Li, L.Y., Li, P., Wang, Y.C., 2022. Modelling of convection, diffusion and binding of chlorides in concrete during wetting-drying cycles. Mar. Struct. 84, In press. https://doi.org/10.1016/j.marstruc.2022.103240.

Liu, Q., Iqbal, M.F., Yang, J., Lu, X., Zhang, P., Rauf, M., 2021. Prediction of chloride diffusivity in concrete using artificial neural network: Modelling and performance evaluation. Constr. Build. Mater. 268, In press. https://doi.org/10.1016/j.conbuildmat.2020.121082.

Liu, Q., Easterbrook, D., Yang, J., Li, L., 2015. A three-phase, multi-component ionic transport model for simulation of chloride penetration in concrete. Eng. Structures 86, 122-133. https://doi.org/10.1016/j.engstruct.2014.12.043.

Liu, Q., Hu, Z., Whang, X., Zhao, H., Qian, K., Li, L., 2022. Numerical study on cracking and its effect on chloride transport in concrete subjected to external load. Constr. Build. Mater. 325, In press. https://doi.org/10.1016/j.conbuildmat.2022.126797.

Lindvall, A., 2003. Environmental actions on concrete exposed in marine and road environments and its response-Consequences for the initiation of chloride induced reinforcement corrosion. PhD Thesis, Chalmers University of Technology, Sweden.

Mainguy, M., 1999. Modèles de diffusion non-linéaires en milieux poreux – Application à la dissolution et au séchage des matériaux cimentaires. PhD. Thesis, Ecole Nationale des Ponts et Chaussées, Paris, France.

Mai-Nhu, J., Machault, M., Semenadisse, J., Ammouche, A., Thauvin, B., 2019a. PN PERFDUB : Résultats des essais de migration des ions chlorures.

Mai-Nhu, J., Rougeau, P., Collin, O., Rozière, E., Cussigh, F., Thauvin, B., Turcry, P., Dierkens, M., Rogat, D., 2019b. French national project "Perfdub" on performance-based approach: Mapping of durability indicators results on extended concrete compositions. In Proceedings of the Fib Symposium 2019: Concrete - Innovations in Materials, Design and Structures, Krakov, Poland, pp. 2014–2021.

Melchers, R.E., 2011. Long-term corrosion of steels exposed to marine environments. Eur. J. Environ. Civ. En. 13:5, 527-546. https://doi.org/10.1080/19648189.2009.9693132.

Moradllo, M.K., Sadati, S., Shekarchi, M., 2018. Quantifying maximum phenomenon in chloride ion profiles and its influence on service-life prediction of concrete structures exposed to seawater tidal zone – A field oriented study. Constr. Build. Mater. 180, 109–116. https://doi.org/10.1016/j.conbuildmat.2018.05.284.

Morris, M.D., 1991. Factorial sampling plans for preliminary computational experiments. Technometrics 33, 161–174. https://doi.org/10.1080/00401706.1991.10484804.

Ohno, M., Limtong, P., Ishida, T., 2022. Multiscale modeling of steel corrosion in concrete based on micropore connectivity. J. Build. Eng. 47, In press. https://doi.org/10.1016/j.jobe.2021.103855.

Othmen, I., Bonnet, S., Schoefs, F., 2018. Statistical investigation of different analysis methods for chloride profiles within a real structure in a marine environment. Ocean Eng. 157, 96–107. https://doi.org/10.1016/j.oceaneng.2018.03.040.

Qu, F., Wengui, L., Dong, W., Tam, V.W.Y., Yu, T., 2021. Durability deterioration of concrete under marine environment from material to structure: A critical review. J. Build. Eng. 35, In press. https://doi.org/10.1016/j.jobe.2020.102074.

Reuge, N., Bignonnet, F., Bonnet, S., 2023. Transport des ions chlorure dans les bétons soumis au marnage : validation d'un modèle physicochimique simplifié. In French, accepted for CFGC AJCE 2023 conference, Paris, France.

Reuge, N., Collet, F., Pretot, S., Moisette, S., Bart, M., Style, O. et al., 2020. Hygrothermal effects and moisture kinetics in a bio-based multi-layered wall: Experimental and numerical studies. Constr. Build. Mater. 240, In press. https://doi.org/10.1016/j.conbuildmat.2019.117928

Sleiman, H., Ouali, A., Aït-Mokhtar, A., 2009. Chloride transport in unsaturated cement-based materials. Eur. J. Environ. Civ. En. 13, 489–499. https://doi.org/10.1080/19648189.2009.9693125.

Soive, A., Tran, V.Q., Baroguel-Bouny, V., 2018. Requirements and possible simplifications for multi-ionic transport models – Case of concrete subjected to wetting-drying cycles in marine environment. Constr. Build. Mater. 164, 799–808. https://doi.org/10.1016/j.conbuildmat.2018.01.015.

Thiery, M., Baroghel-Bouny, V., Bourneton, N., Villain, G., Stéfani, C., 2007. Modélisation du séchage des bétons Analyse des différents modes de transfert hydrique. Rev. eur. génie civ. 11, 541–577. https://doi.org/10.1080/17747120.2007.9692945.

Tian, Y., Wen, C., Wang, G., Hu, J., Mai, Z., 2020. Marine field test for steel reinforcement embedded in mortar: Coupled influence of the environmental conditions on corrosion. Mar. Struct. 73, In press. https://doi.org/10.1016/j.marstruc.2020.102788.

Ta, V.L., Bonnet, S., Kiesse, T.S., Ventura, A., 2016. A new meta-model to calculate carbonation front depth within concrete structures. Constr. Build. Mater. 129, 172–181. http://dx.doi.org/10.1016/j.conbuildmat.2016.10.103.

Tong, L., Xiong, Q. X., Zhang, M., Meng, Z., Meftah, F., Liu, Q., 2023, Multi-scale modelling and statistical analysis of heterogeneous characteristics effect on chloride transport properties in concrete. Constr. Build. Mater. 367, 130096. https://doi.org/10.1016/j.conbuildmat.2022.130096.

Truong, Q.C., El Soueidy, C.P., Li, Y., Bastidas-Arteaga, E., 2022. Probability-based maintenance modeling and planning for reinforced concrete assets subjected to chloride ingress. J. Build. Eng. 54, In press. https://doi.org/10.1016/j.jobe.2022.104675.

Van Genuchten, M.Th., 1980. A closed-form equation for predicting the hydraulic conductivity of unsatured soils. Soil Sci. Soc. Am. J. 4, 892–898. https://doi.org/10.2136/sssaj1980.03615995004400050002x.

Wang, X., 2012. Modélisation du transport multi-espèces dans les matériaux cimentaires saturés ou non saturés et éventuellement carbonatés. Ph.D. Thesis, IFSTTAR, Université Paris-Est., France.

Wang, L., Bao, J., Ueda, T., 2016. Prediction of mass transport in cracked-unsaturated concrete by mesoscale lattice model. Ocean Eng. 127, 144-157. http://dx.doi.org/10.1016/j.oceaneng.2016.09.044.

Wang, Y., Wu, L., Wang, Y., Li, Q., Xiao, Z., 2018. Prediction model of long-term chloride diffusion into plain concrete considering the effect of the heterogeneity of materials exposed to marine tidal zone. Constr. Build. Mat. 159, 297–315. https://doi.org/10.1016/J.CONBUILDMAT.2017.10.083.

Zhang, J., Lounis, Z., 2006. Sensitivity analysis of simplified diffusion-based corrosion initiation model of concrete structures exposed to chlorides. Cement Concrete Res. 36, 1312–1323. https://doi.org/10.1016/j.cemconres.2006.01.015.

Nomenclature

Latin letters

a	Van Genuchten parameter defined in eq. (2) (Pa)
C^*	Normalized chloride concentration defined in eq. (19)
C_b	Binder quantity (kg.m^{-3})
$c_{Cl,f}$	Concentration of free chloride ions (mol.m^{-3} of solution)
$C_{Cl,b}$	Concentration of bound chloride (mol.m^{-3} of material)
$C_{Cl,p}$	Concentration of chloride bound by physisorption (mol.m^{-3} of material)
$C_{Cl,c}$	Concentration of chloride bound by chemisorption (mol.m^{-3} of material)
$c_{Cl,sea}$	Chloride concentration in sea water (mol.m^{-3})
$C_{Cl,tot}$	Total concentration of chloride (mol.m^{-3} of material)
C_{crit}	Critical chloride concentration (wt%/binder)
D_{app}	Apparent diffusion coefficient of chloride ions (m^2.s^{-1})
$D_{v,a}$	Air-vapor binary diffusion coefficient (m^2.s^{-1})
D_{eff}	Effective diffusion coefficient of chloride ions (m^2.s^{-1})
$D_{eff,0}$	Effective diffusion coefficient of chloride ions in water in saturated porous medium (m^2.s^{-1})
ee_i	Elementary effects defined in eq. (20)
es_i	Elementary effects defined in eq. (21)
Hr	Local relative humidity inside the material (-)
J_D	Molar diffusive flux (mol.m^{-2}.s^{-1})
K	Intrinsic permeability (m^2)
k_0	kinetic constant of physisorption (s^{-1})
$k_{r,l}$	Liquid relative permeability (-)
L	Depth of the domain (m)
L_c	Depth of convection (m)
M	Molar mass (kg.mol^{-1})
m	Van Genuchten parameter defined in eq. (2) (-)
n_{eq}	Aluminate equivalent of the material (mol.m^{-3})
P	Pressure (Pa)
P_{atm}	Atmospheric pressure (Pa)

P_c Capillary pressure (Pa)

$P_{v,sat}$ Saturation vapor pressure (Pa)

R Perfect gas constant ($mol^{-1}.K^{-1}$)

RH Ambient relative humidity (-)

S_i Average of es_i

S_i^* Average of $|es_i|$

S_l Degree of saturation (-)

S_{l0} Initial degree of saturation (-)

T Temperature (K)

t Time (s)

t_{crit} Critical time of initiation of corrosion (s)

t_{month} Number of hours in one month (h)

x Cartesian coordinate in the depth of the material (m)

X_i Input parameter

Y Response to the input parameters

Greek letters

α Coefficient defined in eq. (29) (-)

β Parameter defined in eq. (8) (-)

λ Parameter defined in eq. (6) (-)

η Dynamic viscosity ($Pa.s^{-1}$)

γ Freundlich parameter defined in eq. (7) (-)

μ Freundlich parameter defined in eq. (7)

μ_i Average of ee_i

μ_i^* Average of $|ee_i|$

φ Open porosity (-)

ρ Density ($kg.m^{-3}$)

σ_{Si} standard deviation of es_i

$\sigma_{\mu i}$ standard deviation of ee_i

τ Characteristic time of physisorption (s)

Subscripts and superscripts

a	air
b	binder
Cl	Chloride ion
g	Gas phase
l	Liquid phase
v	Water vapor
w	Liquid water